PFC/JA–88–46

# Atomic Hydrogen Density Measurements in the Tara Tandem Mirror Experiment

Guss, W.C, Yao, X.Z. [1], Pócs, L. [2], Mahon, R. [3], Casey, J.,

Horne, S., Lane, B., Post, R.S., Torti, R.P.

Plasma Fusion Center

Massachusetts Institute of Technology

Cambridge, MA 02139

November 1988

This work was supported by U.S. DOE Contract DE–AC02–78ET51013.

[1] Permanent address: Institute of Physics, Beijing, China

[2] Permanent address: Central Research Institute of Physics, Budapest, Hungary

[3] Permanent address: Laser Physics Branch, Naval Research Laboratory, Washington, DC

# Atomic Hydrogen Density Measurements in the Tara Tandem Mirror Experiment

*W.C. Guss, X.Z. Yao†, L. Pócs‡, R Mahon§, J. Casey,*
*S. Horne, B. Lane, R.S. Post, R.P. Torti*
*Plasma Fusion Center, MIT*

## *Abstract*

Neutral and plasma density have been measured in the north well of the central cell of the Tara tandem mirror. The electron plasma density and temperature on the magnetic axis were measured by Thomson scattering to be about $3 \times 10^{12}$ cm$^{-3}$ and 70 eV respectively. The corresponding axial neutral hydrogen density was found to be $1 \times 10^{9}$ cm$^{-3}$, while near the plasma edge at $r = 15$ cm it reached $1 \times 10^{10}$ cm$^{-3}$. The fill gas density at $r \geq 22.5$ cm was $\approx 10^{11}$ cm$^{-3}$. Additional data from secondary electron detectors was used to estimate the radial ion temperature distribution which was found to have about the same width, 12 cm, as the plasma density. The resulting ion pressure profile is peaked compared to the electron pressure profile. Charge exchange losses in the well are found to have a maximum at a radius equal to half the e-folding distance of the plasma density and ion temperature distributions.

## *Introduction*

It is important to understand the interaction of the neutral hydrogen with the plasma hydrogen ions since the neutrals influence both the particle and energy balance of the plasma. The atoms come directly from the fueling process or indirectly from desorption from the wall. As neutrals enter the edge plasma, charge exchange and ionization events occur. Because of the relatively low molecular and atomic ionization energies, most neutrals do not penetrate beyond the edge plasma. A portion do reach the core as charge exchange products or, in the case of hydrogen, as Franck-Condon neutrals. Charge exchange products can leave the plasma from either the core or the edge, and upon striking a wall, generate high-z impurity or additional fuel atoms. In mirror experiments, charge exchange losses dominate the plasma energy balance. Hence, determining their magnitude is important for understanding ion energy loss.

As an example, in EBT[1] molecular hydrogen was a constituent of the edge plasma at high electron temperature as well as being a volume plasma constituent under conditions of low electron density and temperature. Molecular hydrogen was estimated to be approximately $5-10\%$ of the total hydrogen density regardless of the plasma parameters. In an experiment similar to Tara, the RFC-XX-M mirror device[2], also with central cell ICH, the on-axis atomic hydrogen density was measured to be $.15\%$ of the electron density. For other plasmas the same basic phenomena are present although the scale lengths describing the molecular and atomic densities may differ.

Characterizing the neutral gas evolution in Tara was the goal of a program of extensive spectroscopic studies which included passive line-of-sight studies and laser induced resonance fluorescence measurements. Measuring the $H_\alpha$ laser-fluorescence scattering from a plasma is a means of determining the neutral hydrogen density with both spatial and temporal resolution[3]. In addition to being one of the few methods available for determining the neutral density, it is nonperturbing and, when combined with independently measured electron temperature and densities, yields an absolute result. This method has been applied to toroidal plasmas for the study of fueling[4], and impurity evolution[5].

## *Experimental Apparatus*

A portion of the central cell of Tara is shown in Fig. 1 with the axial magnetic field. The central cell is 10 m long with a local field minimum of 2.1

kG, and is bounded by magnetic mirrors with a field of 25 kG. The fueling in Tara is provided by a gas box[6] located near the middle of the central cell and near the top of a local magnetic field maximum (R=2). As a result of the field bump, two magnetic 'wells' are formed in the central cell, each approximately half the central cell in length. Also near the same location is an ICH antenna which launches slow waves with resonances between the gas box and both ends of the central cell[7]. Neutral hydrogen gas flowing out of the gas box must pass through a nearby ICH resonance where it has a high probability of being ionized. As a result, the bulk of the plasma volume is isolated from neutral gas, and the resulting charge exchange losses. Plasma from the central cell flows to the axicell where the electrostatic plugging and thermal barrier potentials are generated. This geometry and plasma startup scenario are unique among thermal barrier tandem mirrors.

A time history of a typical plasma discharge is shown in Fig. 2. Hydrogen gas is initially puffed in $\approx$ 20 ms before the application of ICH power for adequate breakdown. During the discharge, gas is continuously puffed into the gas box. Preionization electrons are supplied by ECRH in one or both of the anchors which are outboard of the central cell. Then plasma breakdown is initiated with the central cell ICH antenna. Because the antenna and gas box are not symmetrically located relative to the magnetic field bump, there is preferential ion heating in the south well and higher neutral pressure in the north well. Plasma development is given by the line density and the diamagnetic loop signals. The axial $H_\alpha$ monitors the line average source function in the plasma core ($r \leq 10$ cm). The neutral gas pressure measurement was made with a fast ionization gauge 139 cm from the central cell gas box toward the laser fluorescence and has a time delay in its response of several milliseconds.

The axial profile of the edge neutral pressure as measured by fast ionization gauges is shown in Fig. 3. The peak in the neutral profile is axially localized around the gas box. The edge pressure at the laser fluorescence location is about a factor of 20 less than at the gas box. In Fig. 4, the Thomson scattering radial profiles of the electron temperature and density are shown for an axial location ($z = 335$ cm) close to the laser fluorescence location ($z = 170$ cm). The density profile monotonically decreases toward the edge from the a value of $\approx 3 \times 10^{12}$ cm$^{-3}$ on the magnetic axis. From a four chord interferometer array, the profile is best fit with a Gaussian with a $12 - 13$ cm scale length. The electron temperature profile increases from $\approx 70$ eV on axis to $\approx 110$ eV on the edge presumably because of the strong edge electron heating from the

central cell ICH. Ion temperatures from the central cell charge exchange in the south well are $T_{i\perp} \approx 1$ keV, and from the swept endloss analyzers, $T_{i||} \approx 150$ eV. For the north well $T_{i\perp}$ is estimated from the ratio of the diamagnetic loop signals in the two wells and is typically $50 - 60\%$ of the south well value. The perpendicular ion temperatures in the north well are lower because of the reduced ion heating in the north resulting from the asymmetric ICH antenna placement, and the ion charge exchange losses as the energetic ions traverse the gas box and the north well. No radial profile information is directly measured for the ion temperature.

The laser fluorescence diagnostic consists of a tunable, flashlamp-pumped dye laser, beam steering optics, detection optics, and both a beam dump and a viewing dump, and are described in more detail elsewhere[8]. Its location at 174 cm is well outside the gas box which extends to about 50 cm. The laser was tuned to the Balmer-alpha line at $6563\mathring{A}$ with a line width of about $0.75\mathring{A}$ which allowed scattering from both the .4 and 4 eV Franck-Condon neutral components. The laser pulse duration was $5\mu$sec. Radial scans were restricted in extent to $r = 15$ cm because of the sizes of both the viewing dump and the large aperture collection lens. This is to be compared with the limiter radius of 22.5 cm. The laser power $1 - 10$ kW cm$^{-2}\mathring{A}^{-1}$ was quite sufficient to saturate the $n = 2$ to $n = 3$ transition so that the fluorescence was not sensitive to the actual value, or to any small fluctuation in, the laser intensity. The problems associated with stray laser light were overcome by using a double pulse technique.

Also at the same location as the laser fluorescence in the north well was a scanning secondary electron detector[9] (SED). Energetic neutral particles from plasma charge exchange events, strike a metal surface, and the resulting secondary electron emission is proportional to the particle energy and flux. Scans were made along chords intersecting at a radius of 70 cm. The signal from this detector can be a result of energetic neutrals causing secondary electron emission or of photoelectron emission from energetic photons. The latter possibility was ruled out through a time history comparison with $H_\alpha$ which would indicate the signal behavior if Lyman series radiation were dominating behavior of the detector.

With the information from a scannable SED, estimates of the radial ion temperature distribution are possible. The SED signal is proportional to the flux of incident charge exchange neutrals and their energy, through the energy dependence of the secondary electron emission coefficient. The radial depen-

dence of plasma density is given by an interferometer array in the south well and the neutral profile is given by the laser fluorescence. The remaining parameter, the charge exchange particle energy, and thus the ion energy, can be inferred.

## *Results*

The ground state neutral population of the neutrals is inferred using the collisional-radiative model of Gohil and Burgess[10]. From the laser fluorescence and Thomson scattering measurements, the neutral density may be inferred. In the interpretation of the laser fluorescence data, the exact electron temperature was not very important because the measured temperatures corresponded to a broad maximum in the hydrogen excitation rate. Radial profiles were made at several times after breakdown when the $H_\alpha$ signal was no longer changing. In a typical discharge, the neutral density profile is hollow (Fig. 4) with the on-axis density about an order of magnitude down from the edge ($r = 15$ cm) density. The profile can be approximated by an edge section with short radial scale length ($2 - 3$ cm) and by a central section with a longer scale length on the order of, or larger than, the plasma radius itself. The short scale length is consistent with room temperature neutrals penetrating an edge plasma with $T_e = 80$ eV and $n_e = .5 \times 10^{12}$ cm$^{-3}$. Neutrals with energy above $\approx 1$ eV are consistent with the longer central scale length. At the largest radial extent ($r = 15$ cm) of the laser fluorescence, the fraction of neutral hydrogen atoms is $2\%$ of the local electron density. On the magnetic axis the fraction is $.04\%$. Fast ionization gauges imply a molecular density of about $2 \times 10^{11}$ cm$^{-3}$ ($r \geq r_p = 22.5$ cm) which is to be compared with a neutral atomic density $\approx 1 \times 10^{10}$ cm$^{-3}$ ($r = 15$ cm) from laser fluorescence. The on-axis neutral density time history is shown in Fig. 5. The radial scale length of the molecular species was not measured.

Our results differ from those observed on the RFC-XX-M experiment. The central atomic fraction ($.15\%$) and the center to edge neutral ratio (1:5) differ from RFC-XX-M which had a substantially lower ($T_e = 30$ eV) and flatter electron temperature. Electron line densities are comparable at $.5 - 1 \times 10^{14}$ cm$^{-2}$ for both experiments.

The radial distribution of the ion energy was determined by reconstructing the SED chord averaged signals according to an integral over the local charge

exchange rate assuming cylindrical symmetry

$$V_{SED} = k \int_{-d(r)}^{d(r)} \dot{n}_o(r)\gamma_e \, dl$$
$$= k \int_{-d(r)}^{d(r)} n_o(r) n_i(r) \langle \sigma v \rangle_{cx}(r) \gamma_e \, dl$$

where $k$ is a proportionality constant, $n_o, n_i$ are the neutral atom and ion densities, $\langle \sigma v \rangle_{cx}$ is the Maxwellian averaged charge exchange rate, and $\gamma_e$ is the secondary electron coefficient of the detector surface. The integral is performed along the chord of length $2d$ where $d$ is a function of the chord radial location. The ion energy dependence[9] is primarily in the secondary electron coefficient ($T_i^8$) but also weakly[11] in the charge exchange rate ($T_i^{1/3}$). Numerically integrating over the known radial dependences along the line of sight with the assumed radial dependence of the ion energy yields a quantity that is compared to the measured SED signal. In Fig. 6 the profile of the chord averaged SED data at 20 ms is compared to computed values assuming Gaussian ion temperature profiles with scale lengths about the same as the plasma density. Ion temperature profiles with assumed scale lengths differing by more than 1 cm gave significantly poorer fits to the data.

With the determination of the ion temperature profile, the radial dependence for charge exchange losses can be computed for the north well. The ion temperature in the north well was inferred from the south well charge exchange measurement by comparing the diamagnetic loop signals at the two locations and assuming that the same radial ion temperature profiles. A typical charge exchange spectrum constructed from a 30 ms sweep during a discharge is shown in Fig. 7. Under conditions of moderate density, the distribution can be reasonably well described by a single temperature, and the unfolding of the ion temperature profile by the above equations is accurate without resorting to an ion energy distribution. For the standard Tara running conditions, the radial charge exchange losses per unit axial distance are shown in Fig. 8. Maximum charge exchange loss occurs at a radius of $\approx 6$ cm which is about half the scale length of the ion temperature and plasma density profiles. The location of the maximum is a function of the increasing plasma volume near the axis and the rapidly decreasing ion temperature toward the plasma edge. The magnitude of the total charge exchange losses would be larger than what is calculated for the well because of the sharply peaked axial neutral pressure profile (Fig. 3).

Detailed information for the gas box is not available, however if the profiles and the ion temperatures are comparable, the charge exchange losses there are at least a factor of twenty larger because of the larger neutral pressure. The losses in the south well scale as the average ion temperature and are about a factor of two larger assuming the atomic hydrogen density scales with the edge molecular density. Using the value for the charge exchange losses in the north well and scaling it to the edge neutral density, ion temperature, and plasma density a lower limit to the total central cell charge exchange losses can be obtained. It is a lower limit because the neutral density profile in the gas box is expected from axial TV scans to be much more uniform radially than in the well, and the charge exchange losses consequently larger. Because of the presence of the central cell divertor, direct laser fluorescence measurements were not possible in this important region. Integrating axially using the well profiles yielded a total central cell charge exchange loss of 40 kW. Golovato, *et al.*[7] make a separate determination of the total charge exchange losses from the total gas input, the measured gas efficiency, and the observed endloss. Their value is 60 kW for discharges with slightly higher gas puff rate and is comparable to our more direct measurement.

It is also possible to calculate the radial pressure profiles. Figure 9 shows the ion and electron pressure profiles and the total pressure profile for the north well. The ion pressure profile is much more peaked than the electron profile with e-folding radii of $\approx$ 8 cm and $\approx$ 13.5 cm respectively. Measurements of the ICH wave magnetic field[7] amplitude show a peak within $r = 10$ cm. Although the magnetic fields can not be used to specify the location of the plasma heating, the present results suggest that the large wave magnetic fields may be associated with ion heating.

## *Conclusions*

A laser fluorescence diagnostic on the Tara tandem mirror has measured the scattered resonant Balmer-alpha radiation from Franck-Condon and low energy charge exchange products. Radial profiles were taken at two times for which the axial $H_\alpha$ light indicated steady state conditions had been reached. Measurements show very similar profiles with a factor of ten attenuation of the the neutral density between the plasma edge and the axis. Most of the attenuation occurs near the plasma edge where the neutral profile gradient scale length is 2-3 cm. The neutral density time history shows that conditions are relatively constant during the discharge. The radial profile scale lengths are

consistent with the ionization of room temperature neutrals at the plasma edge and at least 1 eV neutrals in the plasma core.

The ion temperature profile inferred from laser fluorescence and SED measurements is well described by a Gaussian and has about the same width as the plasma density. Charge exchange losses in the north well have a local maximum at a radius about half the plasma density and ion energy scale length. The ion pressure is localized near the axis and is narrower than the electron pressure profile. The inferred total central cell charge exchange losses have been determined and are comparable to indirect estimates from endloss measurements.

*Acknowledgements*

This work was supported by U.S. DOE Contract DE-AC02-78ET51013.

†Permanent Address: Institute of Physics, Beijing, China

‡Permanent Address: Central Research Institute of Physics, Budapest, Hungary

§Permanent Address: Laser Physics Branch, Naval Research Laboratory, Washington, D.C.

## References:


[1]J.C. Glowienka, and R.K. Richards, J. Plasma Physics, **35**, 519(1986)

[2]K. Muraoka, K. Uchino, Y. Itsumi, M. Hamamoto, M. Meada, M. Akazaki,T. Kawamoto, R. Kumazazwa, S. Okamura, K. Adati, T. Aoki, H. Fujita, K. Hattori, S. Hidekuma, Y. Okubo, T. Sato, H. Garner, D.R. Baker, and H.D. Price, Jpn. J. Appl. Phys. **24**, L59(1985)

[3]V.B. Burakov, P. Ya. Misyakov, P.A. Naumenko, S.V. Nechaev, G.T. Razdobarin, V.V. Semenov, L.V. Sokolova, and I.P. Folomkin, JETP Lett. **26**, 403(1977)

[4]P. Bogen, and E. Hintz, Comm. Plasma Phys. Contr. Fusion **4**, 115(1978)

[5]B. Schweer, D. Rusbueldt, and E. Hintz, J. Nucl. Mater. **93**, 357(1980)

[6]R.S. Post, K. Brau, S. Golovato, E. Sevillano, D.K. Smith, W. Guss, J. Irby, R. Myer, and J. Sullivan, Nucl. Fusion **27**, 217(1987)

[7]S.N. Golovato, K. Brau, J. Casey, J. Coleman, M.J. Gerver, W. Guss, G. Hallock, S. Horne, J. Irby, R. Kumazawa, J. Kesner, B. Lane, J. Machuzak, T. Moran, R. Myer, R.S. Post, E. Sevillano, D.K. Smith, J.D. Sullivan, R. Torti, L.Wang, Y. Yasaka, X.Z. Yao, and J. Zielinski, Submitted to Phys. Fluids

[8]W.C. Guss, X.Z Yao, L. Pócs, R Mahon, and J. Casey, and R.S. Post, Rev. Sci. Instrum. **59**, 1470(1988)

[9]J.A. Ray, and C.F. Barnett, J. Appl. Phys., **42**, 3260(1971)

[10]P. Gohil, and D.D. Burgess, Plasma Phys. **25**, 1149(1983) and by private communication with P. Gohil, General Atomics

[11]R.L. Freeman, and E.M. Jones, Culham Laboratory Report CLM-R 137, 1974

## Figure Captions:

FIG. 1. Tara central cell and axial magnetic field with slot antenna and gas box. The laser fluorescence diagnostic is 167 cm from the midplane.

FIG. 2. Typical discharge with fast ion gauge (z=139 cm) (a), line density (b), cental cell diamagnetism (c), and ICH slot antenna pulse (d). Turn-on of the ICH defines t=0.

FIG. 3. Axial neutral gauge pressure profile in the central cell at 8 ms.

FIG. 4. Radial profiles of laser fluorescence inferred $n_o$ (a), which was reduced from the raw fluorescence data taken at $z = 167$ cm (b), using the Thomson scattering $T_e$ (c), and $n_e$ (d) taken at $z = 335$ cm.

FIG. 5. The on-axis neutral density $n_o(0)$ was measured as a function of time during the discharge.

FIG. 6. radial dependence of inferred SED signals for different assumed ion energies.

FIG. 7. Charge exchange spectrum for the south well ($z = -167$ cm) with a $T_{i\perp} = 1150 \pm 200$ eV.

FIG. 8. Charge exchange losses from a 1 cm shell per unit axial length as a function of radius (o) and radial summed ($\triangle$) at 8 ms.

FIG. 9. Ion, electron, and total pressures for the north well.

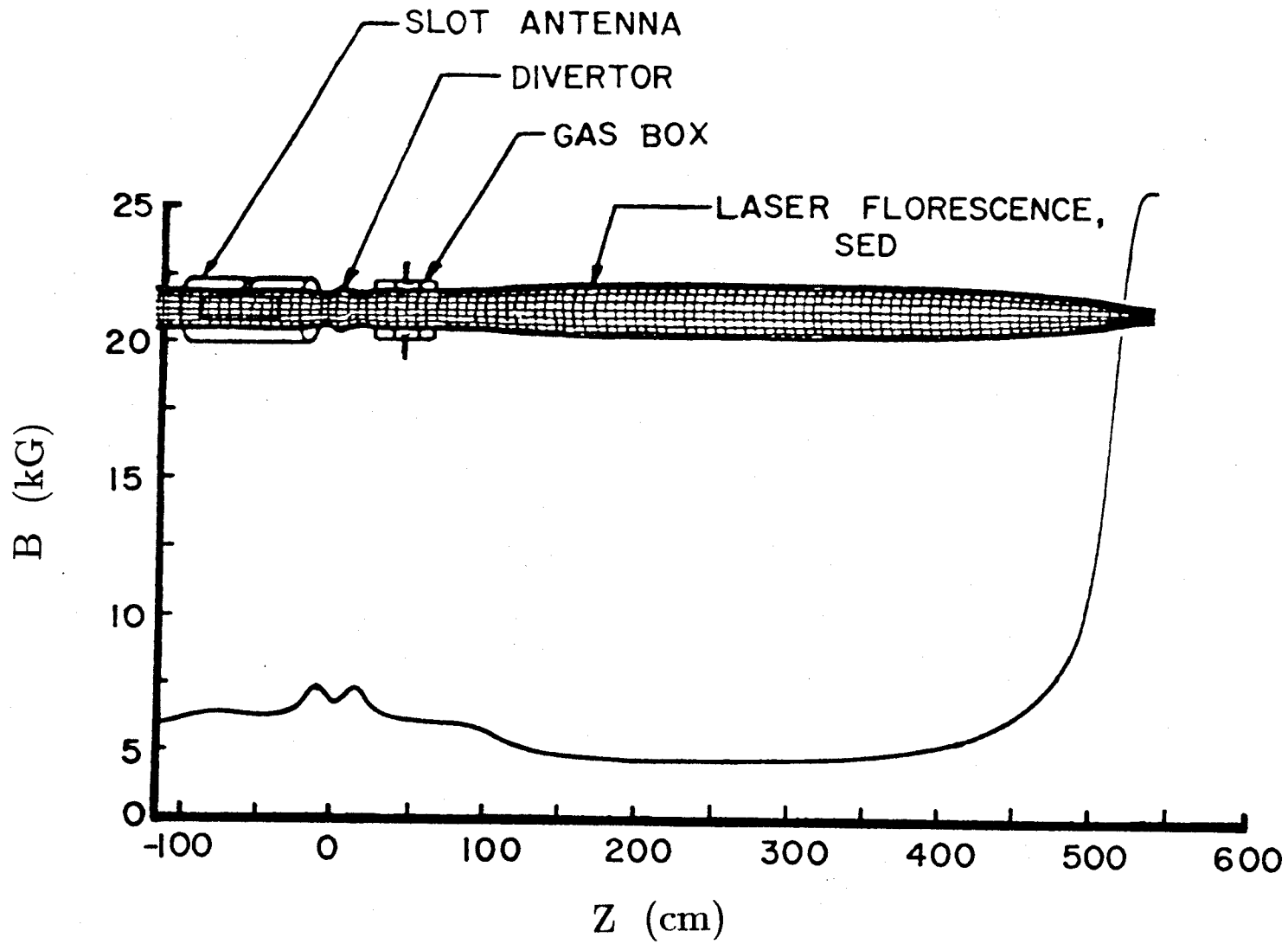
SLOT ANTENNA
DIVERTOR
GAS BOX
LASER FLORESCENCE, SED
B (kG)
25
20
15
10
5
0
-100
0
100
200
300
400
500
600
Z (cm)

Figure 1

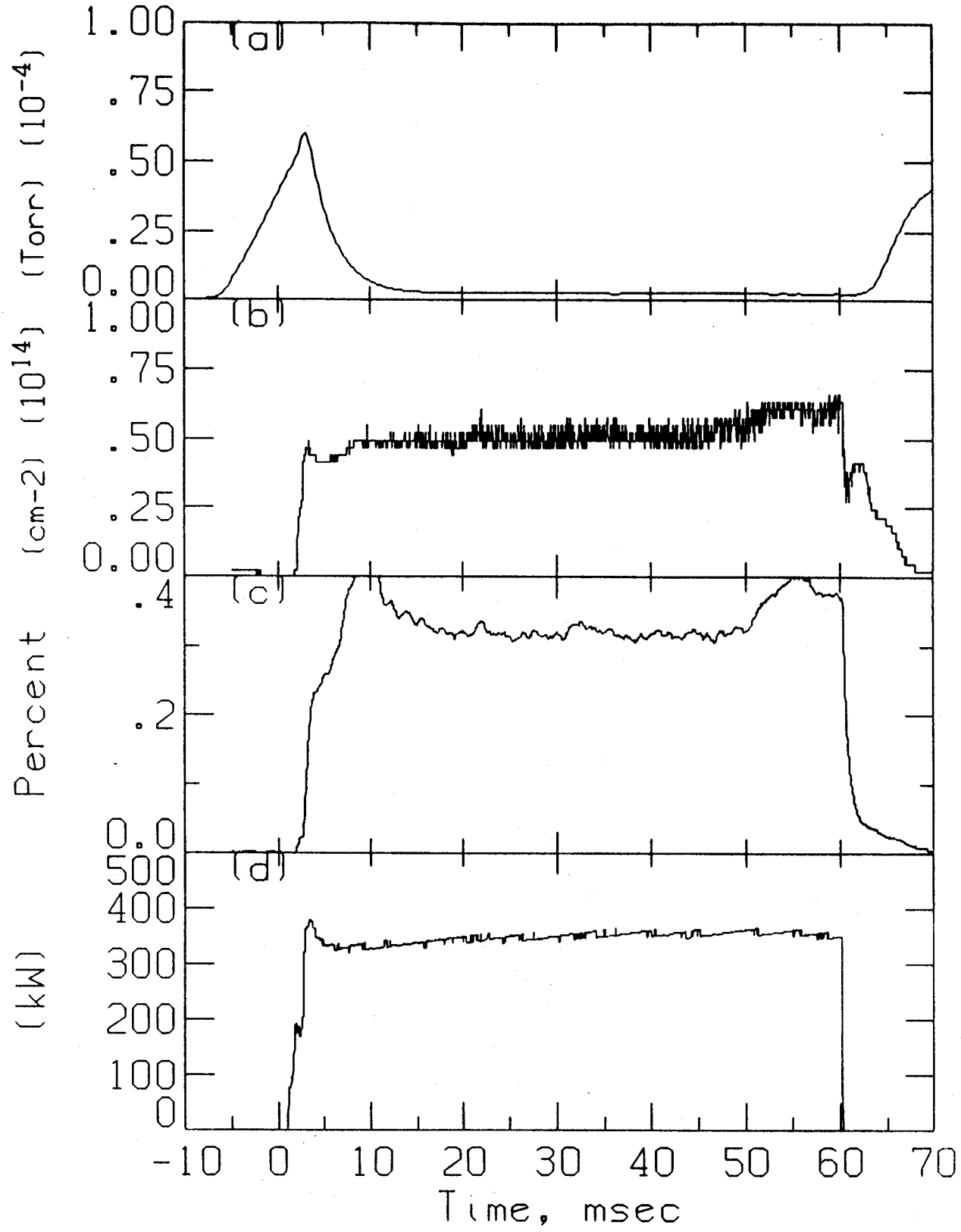
(a)
(b)
(c)
(d)
1.00
.75
.50
.25
0.00
1.00
.75
.50
.25
0.00
.4
.2
0.0
500
400
300
200
100
0
Percent (cm-2) (10^14) (Torr) (10^-4)
(kW)
-10
0
10
20
30
40
50
60
70
Time, msec

Figure 2

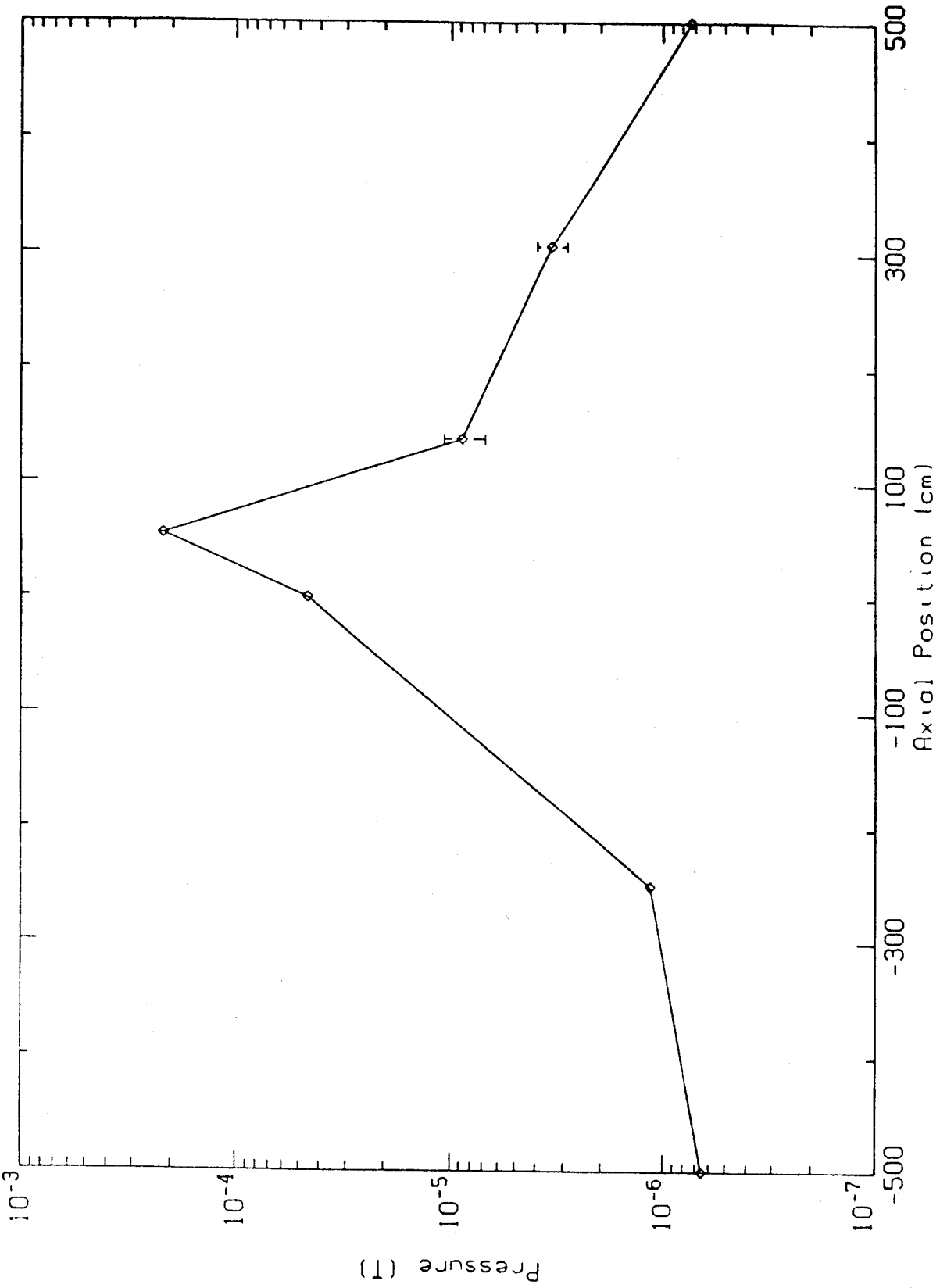
Pressure (T)
10^-3
10^-4
10^-5
10^-6
10^-7
-500
-300
-100
100
300
500
Axial Position (cm)

Figure 3

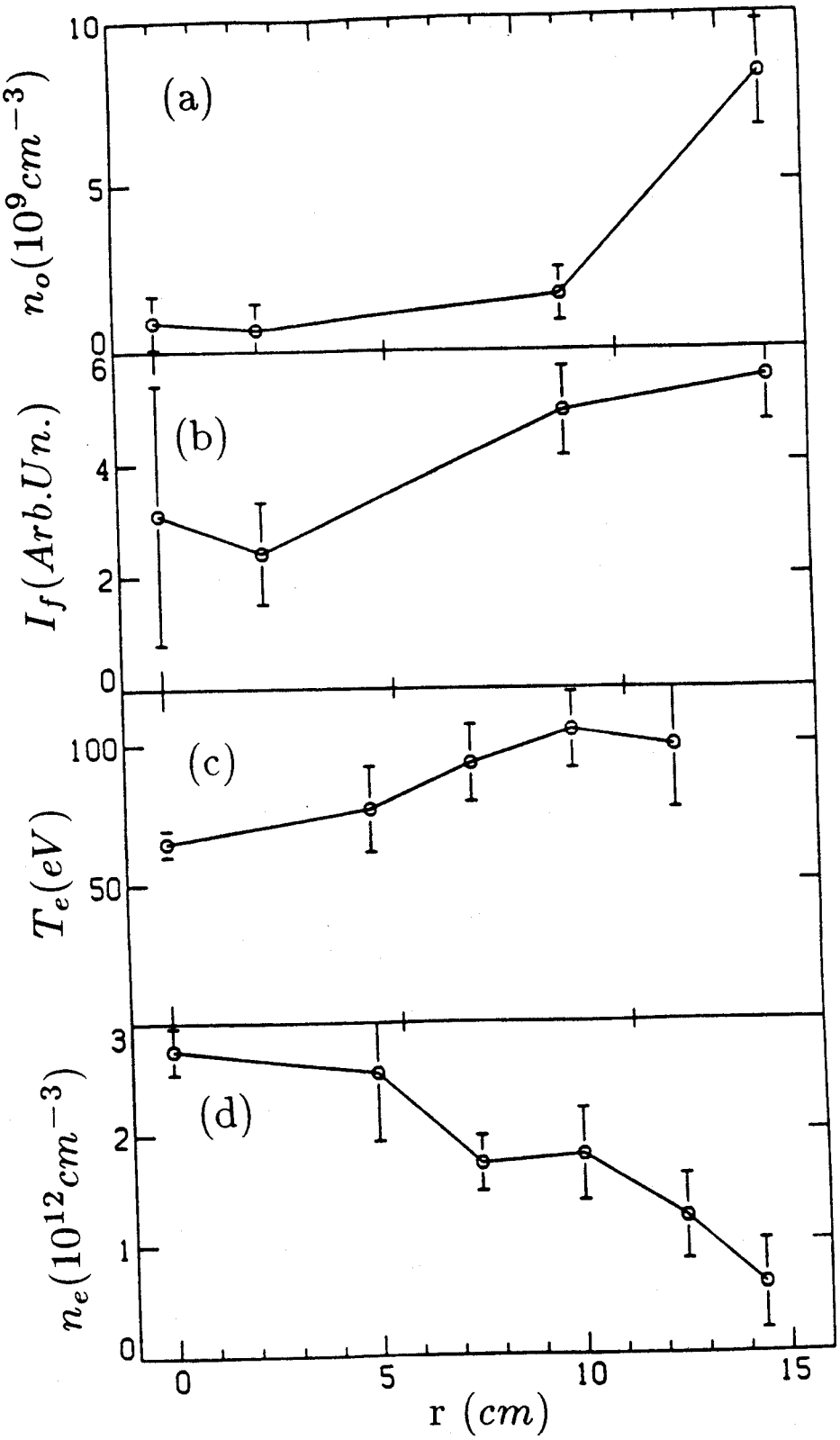


Figure 4

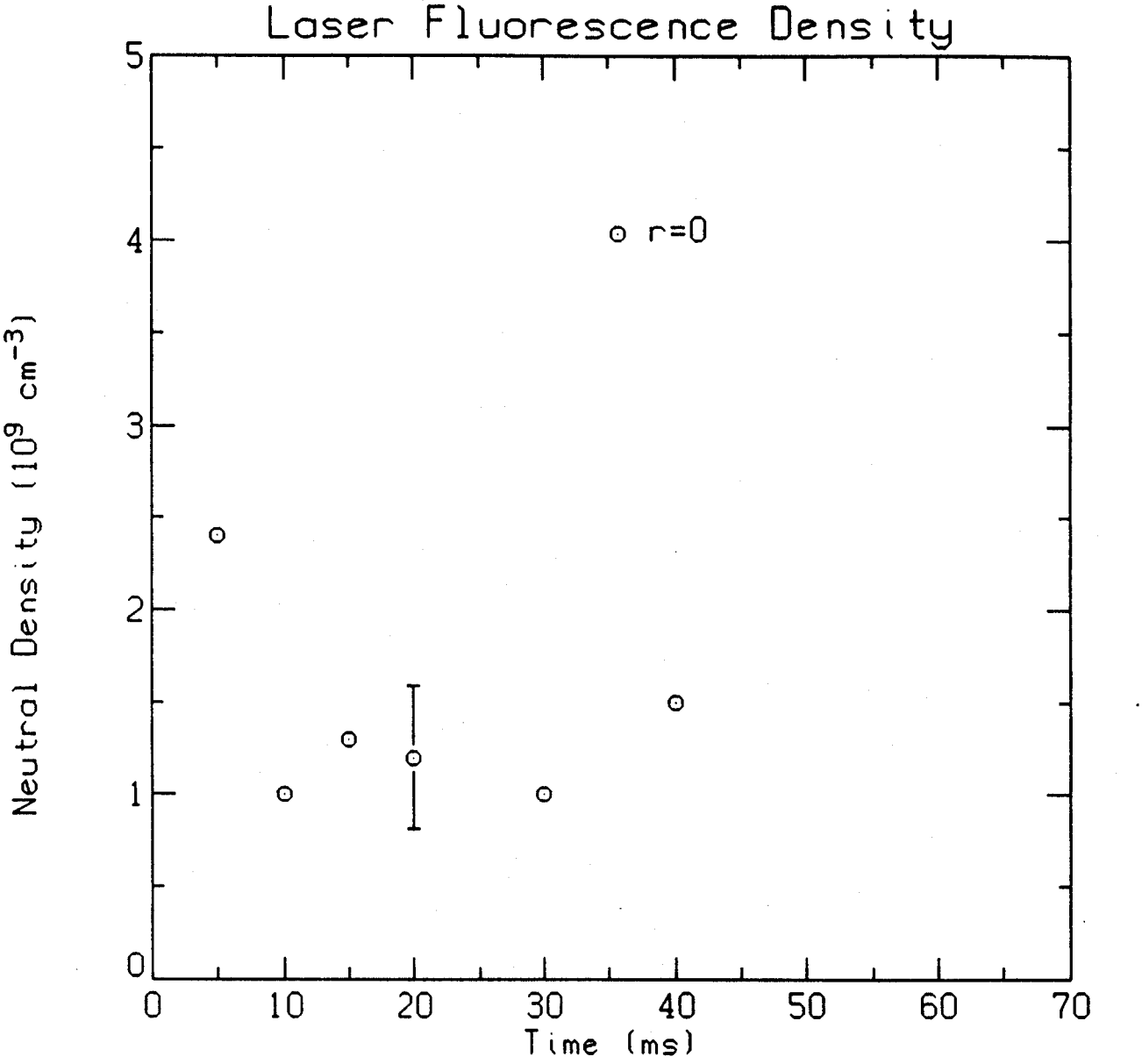
Laser Fluorescence Density
r=0
Neutral Density ($10^9$ cm$^{-3}$)
Time (ms)
0
1
2
3
4
5
0
10
20
30
40
50
60
70

Figure 5

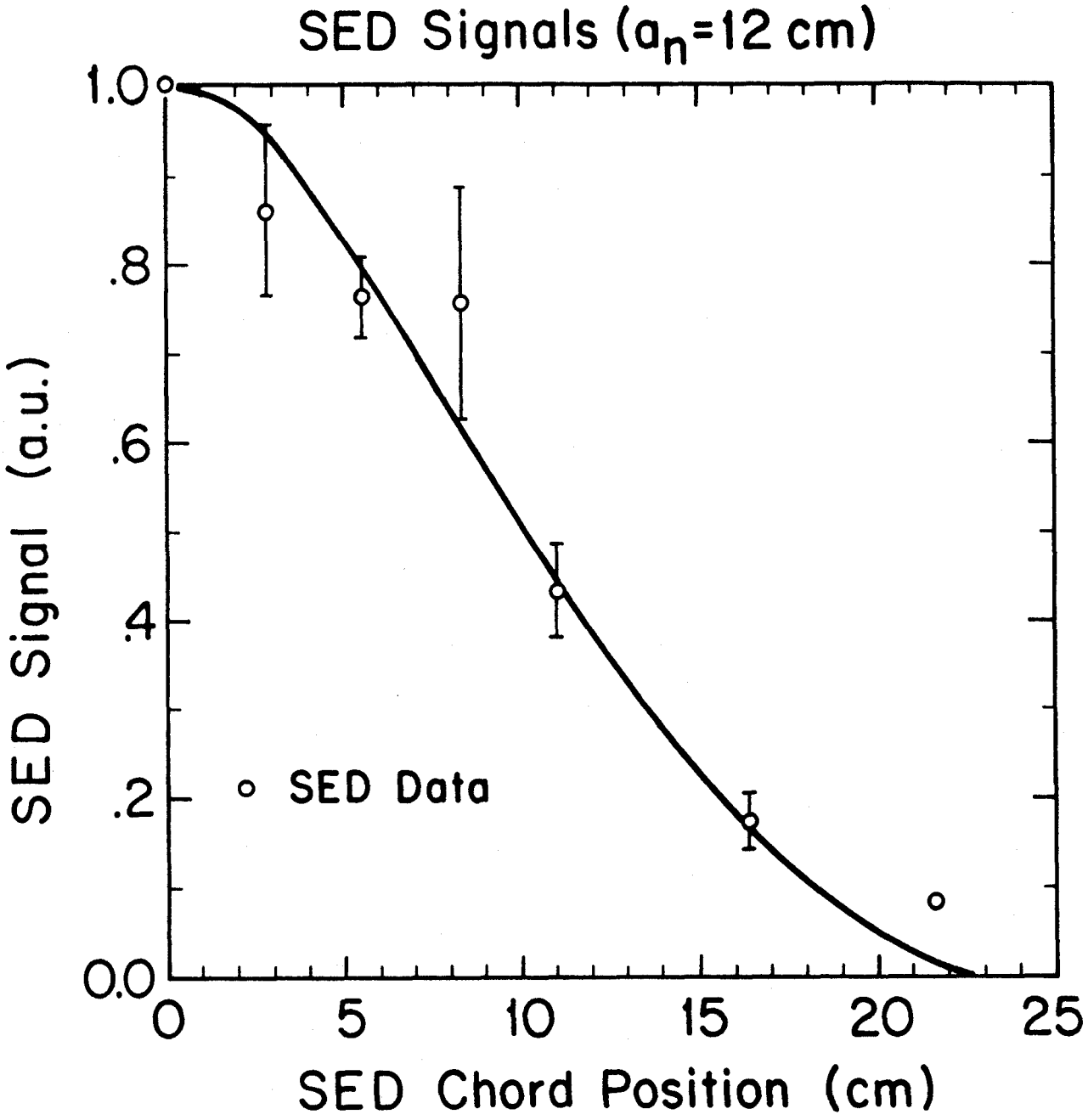
SED Signals ($a_n$=12 cm)
1.0
.8
.6
.4
.2
0.0
SED Signal (a.u.)
SED Data
0
5
10
15
20
25
SED Chord Position (cm)

Figure 6

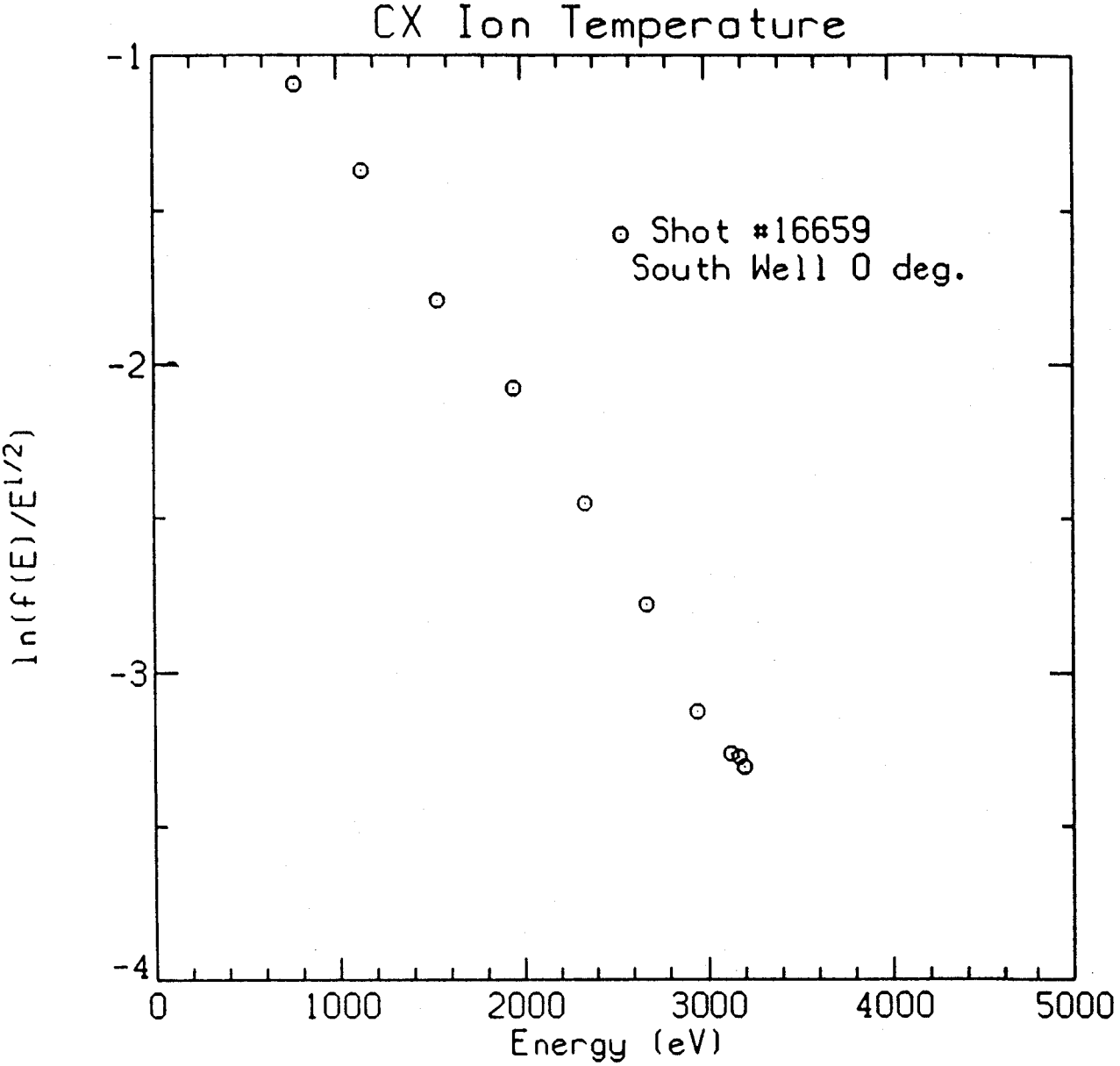
CX Ion Temperature
Shot #16659
South Well 0 deg.
ln(f(E)/E^1/2)
-1
-2
-3
-4
0
1000
2000
3000
4000
5000
Energy (eV)

Figure 7

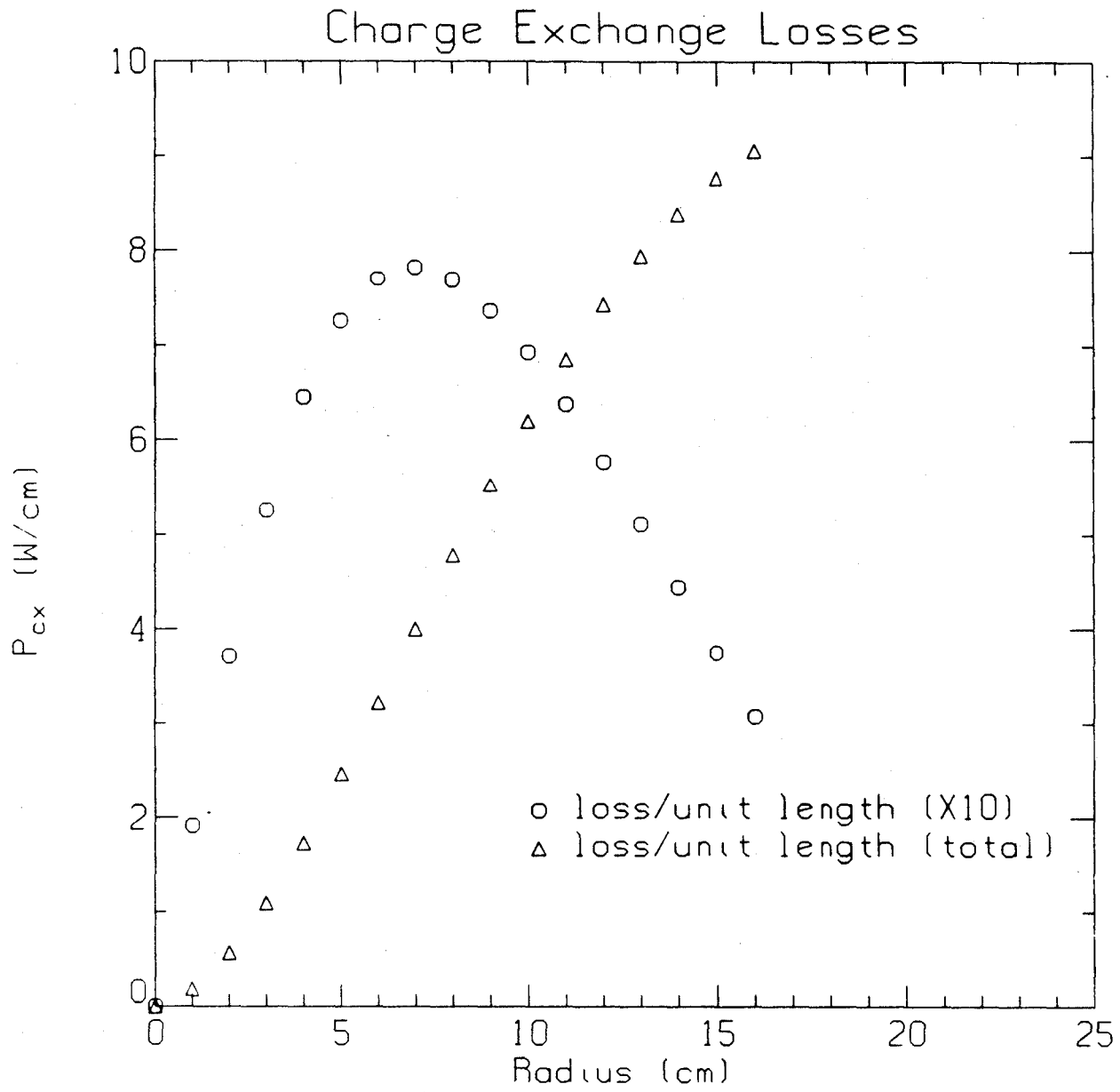
Charge Exchange Losses
10
8
6
4
2
0
0
5
10
15
20
25
Radius (cm)
$P_{cx}$ (W/cm)
o loss/unit length (X10)
Δ loss/unit length (total)

Figure 8